J Nondestruct Eval (2012) 31:90–98
DOI 10.1007/s10921-011-0124-6

Characterization of Cast Iron Microstructure Through Fluctuation and Fractal Analyses of Ultrasonic Backscattered Signals Combined with Classification Techniques

E.P. de Moura · P.G. Normando · L.L. Gonçalves · S.E. Kruger

Received: 4 May 2011 / Accepted: 21 November 2011 / Published online: 6 December 2011

Abstract This work aims at evaluating the performance of pattern recognition methods in the identification of different microstructures presented by cast iron, namely, lamellar, vermicular and nodular microstructures, through the statistical fluctuation and fractal analyses of backscattered ultrasonic signals. The signals were obtained with a broad band ultrasonic probe with a central frequency of 5 MHz. The statistical fluctuations of the ultrasonic signals were analyzed by means of Hurst (RSA) and detrended-fluctuation analyses (DFA), and the fractal analyses were carried out by applying the minimal cover and box-counting techniques to the signals. The curves obtained from the statistical fluctuations and fractal analyses, as functions of the time window, were processed by using four pattern classification techniques, namely, principal-component analysis (PCA), Karhunen-Loève transformation (KLT), neural networks and Gaussian classifier. The best results were obtained by Karhunen-Loève expansion and neural networks, where an approximately 100% success rate has been reached for the classification of the different microstructures as well as for the training and the testing sets of events. The results presented correspond to an average taken over 100 randomly chosen sets of events. These results indicate that, within the techniques used, the Karhunen-Loève transformation and neural network associated with the statistical fluctuation analyses (RSA and DFA) are the best tools for the recognition of the different cast iron microstructures. It is worthwhile pointing out that the microstructure classification was made by using backscattering signals acquired during pulse echo ultrasonic nondestructive testing only. Therefore, that approach is a promising method for material characterization.

Keywords Nondestructive testing · Cast iron · Statistical fluctuation analysis · Fractal analysis · Principal component analysis · Karhunen-Loève transformation · Neural network · Gaussian classifier

E.P. de Moura (✉) · P.G. Normando · L.L. Gonçalves
Departamento de Engenharia Metalúrgica e de Materiais, Universidade Federal do Ceará, Campus do Pici, Bloco 714, 60440-554, Fortaleza, Ceará, Brazil
e-mail: elineudo@ufc.br

S.E. Kruger
Institut des Matériaux Industriels, Conseil National des Recherches, 75 Boul. de Mortagne, Boucherville, Quebec J4B 6Y4, Canada

1 Introduction

The nondestructive characterization of materials enables great applications in many industrial fields. Ultrasonic velocity and attenuation in plane parallel specimens are obtained by using a pulse-echo technique that measures the amplitude variation as a function of the transit time in backwall echoes. The obtained information has been widely used for materials characterization [1, 2], but it is limited and specific. However, as an incident acoustic signal propagates within the material, it is scattered by the microstructure yielding a very noisy signal. These backscattered signals have been shown to contain useful information of the microstructure and its spatial distribution [3]. They show a highly irregular structure and in order to study them, as a means to characterize materials, one needs nonconventional statistical methods. Traditional approaches such as power spectrum analysis present some difficulties when one wants

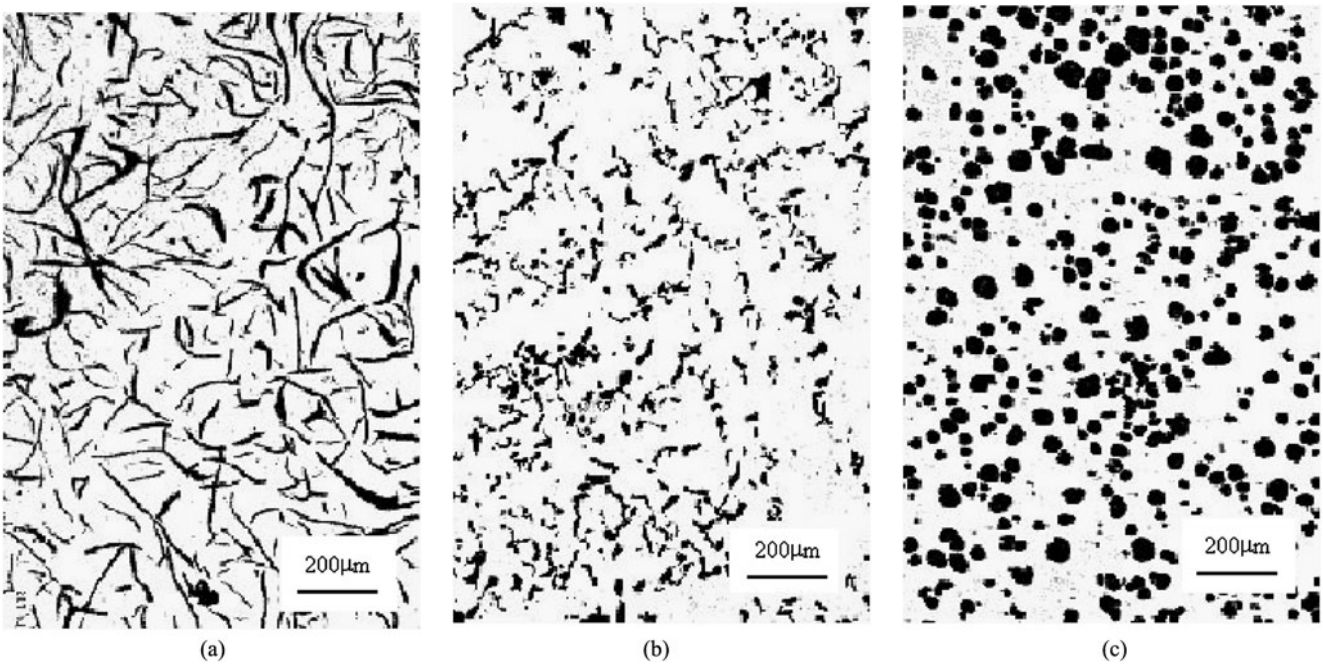

Fig. 1 Micrograph of cast iron samples analyzed. (**a**) lamellar, (**b**) vermicular, (**c**) nodular

to quantify more precisely long-range correlations in non-stationary signals [4].

In this work we have applied the statistical fluctuation analyses (classical rescaled range analysis (RS) [5] and detrended fluctuation analysis (DFA) [6]) and fractal analyses (minimal cover analysis [7] and boxcounting analysis [8]) associated with pattern recognition techniques (principal component analysis [9], Karhunen-Loève transformation [9], neural network [10, 11] and Gaussian classifier [9]) to study ultrasonic backscattered signals from three different samples of cast iron: nodular, lamellar and vermicular graphite. It corresponds to an extension of a previous work of Matos et al. [3], which was restricted to the statistical fluctuation analysis by using RS and DFA. These types of analysis have been widely used in the study of random non-stationary series ranging from seismic [12] and climate data [13], to wind speed [14] and financial data [15], as well as in the study of different music genres [16]. Their use in the characterization of acoustic signal has been introduced by Dutta and Barat [17] in the analysis of ultrasonic backscattered signals obtained in the study of single crystal and polycrystalline materials.

The outline of this paper is as follows. In Sect. 2 the experiment is summarized. In Sect. 3 the algorithms of the rescaled range analysis, detrended fluctuation analysis, minimal cover and boxcounting methods are reviewed. The pattern recognition methods are presented in Sect. 4. The results and discussion are presented in Sect. 5 and in Sect. 6 we summarize the main conclusions.

2 Material and Methods

Cast iron is a family of material widely used which presents precipitated graphite particles with a different morphology embedded in an iron matrix. The high carbon and silicon contents in the cast iron are responsible for produce lamellar or flake graphite as displayed in Fig. 1(a). This kind of cast iron is called grey cast iron. Cerium and magnesium additions degenerate the lamellar graphite producing nodular or spheroidal graphite. This cast iron is known as ductile iron and is illustrated in Fig. 1(c). Furthermore, it is possible produce vermicular cast iron (also known as compacted graphite iron) which have graphite in an intermediate shape between spheroidal and flake and most of its properties lie in between those of grey and ductile iron (see Fig. 1(b)) [18–21].

Each cast iron sample has been prepared following the typical specimen preparation procedure (sectioning, grinding, polishing and etching) [22]. Cast iron samples with dimensions 430 mm × 550 mm × 620 mm were cut and machined. Etching with 2% Nital was used to reveal graphite as dark regions in the micrographs. Each specimen was characterized by quantitative metallography for particle diameter, sphericity and particle number density. Figure 1 shows representative micrographs of lamellar (flake), vermicular (compacted) and nodular (spheroidal) graphite assessed by optical microscopy and studied in this work.

Sample preparation procedure for metallography involves time and is destructive. For this reason, samples of

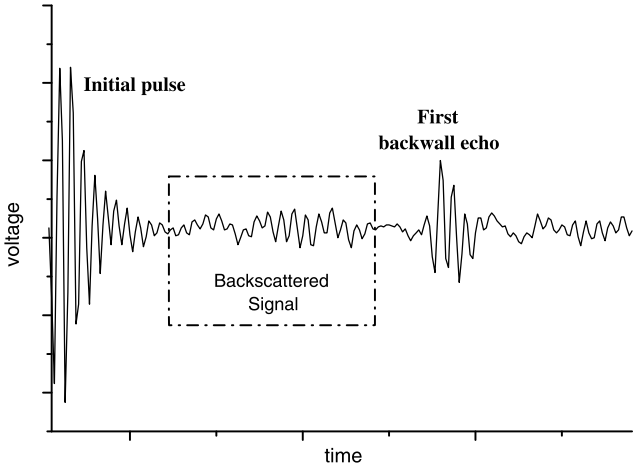

Fig. 2 Typical time-domain ultrasonic signal with backscattered portion highlighted

each cast iron have been submitted to nondestructive evaluation. Figure 2 show a typical ultrasonic signal acquired by pulse-echo technique. Only the part between the initial pulse and the first backwall echo, called backscattered signal, was analyzed in this work. The main advantage of using backscattered signal is that backwall echo or parallel surfaces of inspection are not needed. Interfaces between media with different acoustic impedance (precipitates of second phase or grain boundaries) behave as scattering centers. Acoustic impedance is defined as the product of density and velocity of propagation, $\Delta\rho v$. Besides the acoustical impedance, the scatterer size-to-wave-length ratio (a/λ) plays a key role in the nature and magnitude of scattering [2].

In order to obtain the backscattered signals for statistical fluctuation and fractal analyses a broad band ultrasonic probe with central frequency of 5 MHz was used. Cast iron in general, and lamellar cast iron in particular, are materials with high coefficient of attenuation. Frequency values higher than 5 MHz are greatly attenuated and yield low signal/noise ratios. Therefore, in order to allow a larger band of frequencies we have chosen a broad band probe with central frequency of 5 MHz for the different cast irons. The signals were recorded by positioning the probe on each sample in 40 different positions randomly chosen, and a backscattered signal of 512 points was recorded at each position at a sampling rate of 40 M samples/s.

3 Statistical Fluctuation and Fractal Analyses

The following subsections describe the methods of fluctuation and fractal analyses employed as a preprocessing step in the microstructure classification scheme. These methods are usually employed to identify long-term memory effects in self-affine (or fractal) time series. In a time series of genuine fractal nature, memory effects can be gauged by a single number η which relates a measure of the average fluctuations $Q(\tau)$ inside the time series to the size τ of the time window used in the calculation, according to the power law

$$Q(\tau) \sim \tau^{\eta}. \tag{1}$$

For experimental time series, which of course cannot be genuinely fractal, the various analyses described below have proved to be nevertheless quite useful in providing signatures of the underlying processes peculiar to distinct situations, such as different defects present in welding joints probed by ultrasonic techniques [23], as well as different defects in gearboxes as registered by vibration signals [24].

Each technique involves the calculation of the average of the functions $Q(\tau)$ over all cells, for a defined set of values of τ, which will be used to characterize the different microstructures since the exponents η solely are not sufficient to produce the desired discrimination.

3.1 Hurst (or R/S) Analysis

The rescaled-range (R/S) analysis was introduced by Hurst [5] as a tool for evaluating the persistence or antipersistence of a time series. The method works by dividing the series into intervals of a given size τ, and calculating the average ratio R/S of the range (the difference between the maximum and minimum values of the series) to the standard deviation inside each interval. The size τ is then varied, and a curve of the rescaled range R/S as a function of τ is obtained.

Mathematically, the R/S analysis is defined in the following way. Given an interval of size τ, whose left end is located at point i_0, the average of the time series z_i inside the interval is calculated as,

$$\langle z\rangle_{\tau} = \frac{1}{\tau}\sum_{i=i_0}^{i_0+\tau-1} z_i. \tag{2}$$

It is then defined an accumulated deviation from the mean as

$$z_i = \sum_{k=i_0}^{i}(z_k - \langle z\rangle_{\tau}) \tag{3}$$

from which the range

$$(\tau) = \max_{i_0\le i\le i_0+\tau-1} z_i - \min_{i_0\le i\le i_0+\tau-1} z_i, \tag{4}$$

and the corresponding standard deviation

$$S(\tau) = \sqrt{\frac{1}{\tau}\sum_{i=i_0}^{i_0+\tau-1}(z_k - \langle z\rangle_{\tau})^2} \tag{5}$$

are extracted.

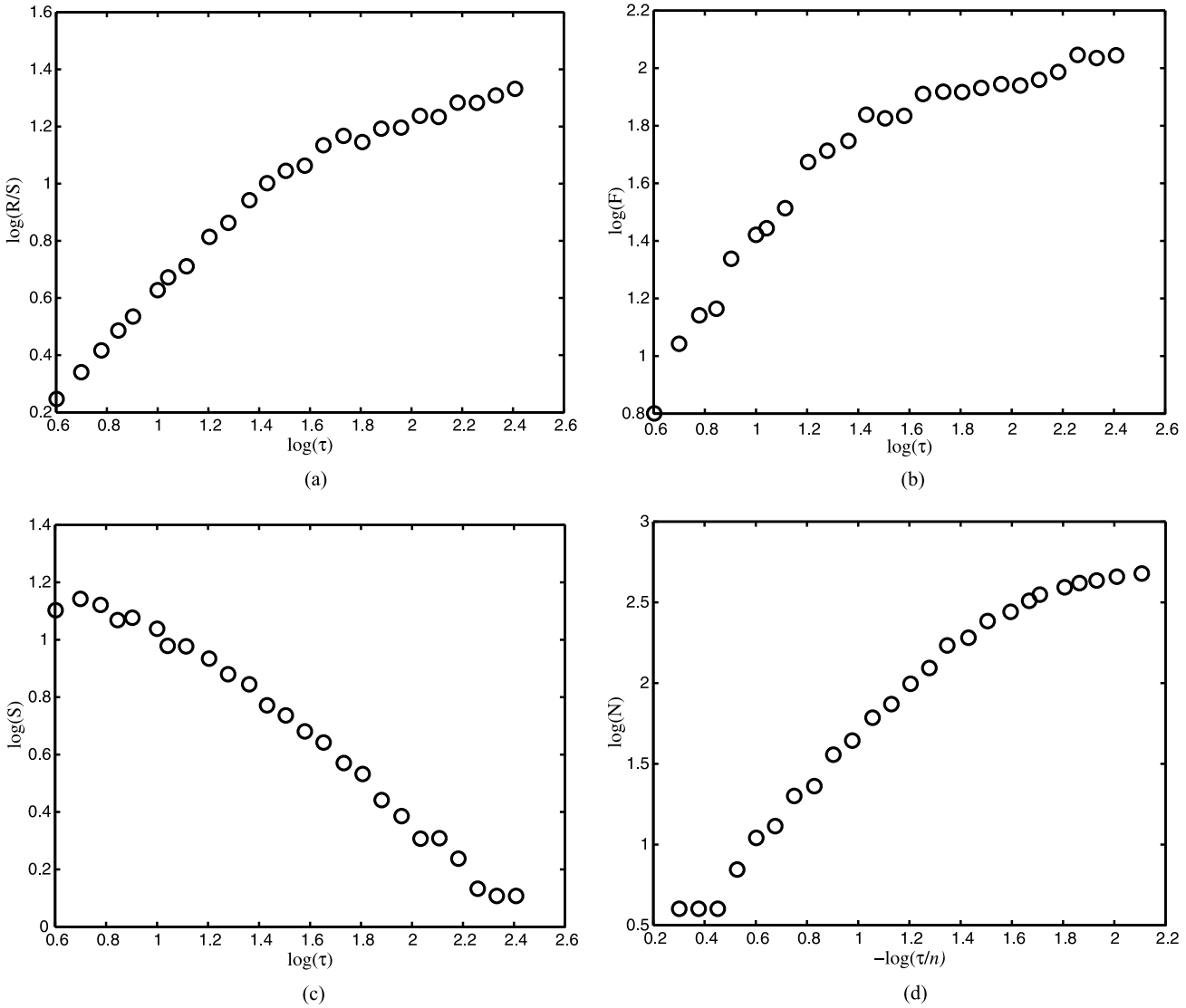

Fig. 3 Typical curves for the various statistical and fractal methods. (**a**) Hurst analysis, (**b**) detrended-fluctuation analysis, (**c**) minimal cover analysis, (**d**) box-counting analysis

Finally, the rescaled range $R(\tau)/S(\tau)$ is obtained, as well as its average over all intervals. In a curve with true fractal features, the rescaled range should satisfy the scaling form

$$\frac{R(\tau)}{S(\tau)} \sim \tau^H, \tag{6}$$

where H is the Hurst exponent.

A typical curve obtained from the Hurst analysis of a signal is shown in Fig. 3(a).

3.2 Detrended-Fluctuation Analysis

The detrended-fluctuation analysis (DFA) [6] aims at improving the evaluation of correlations in a time series by eliminating trends in the data. The method consists initially in obtaining a new integrated series

$$\tilde{z}_i = \sum_{k=1}^{i} (z_k - \langle z \rangle) \tag{7}$$

the average being taken over all n points,

$$\langle z \rangle = \frac{1}{n} \sum_{i=1}^{n} z_i. \tag{8}$$

After dividing the series into L ($L = \text{int}[n/\tau]$) intervals of size τ, the points inside a given interval are fitted by a straight line. Then, for eliminating linear trends a detrended-variation function $\Delta_i(\tau)$, for each interval τ is obtained by subtracting from the integrated date the local trend as given

by the linear fit. The detrended-variation function is explicitly defined as

$$\Delta_i(\tau) = \tilde{z}_i - h_i(\tau), \tag{9}$$

where $h_i(\tau)$ is the value associated with point i according to the linear fit. Finally, the root-mean-square fluctuation $F(\tau)$ inside an interval can be calculated as

$$F(\tau) = \sqrt{\frac{1}{\tau}\sum_i \Delta_i^2(\tau)}. \tag{10}$$

For a true fractal function, $F(\tau)$ should behave as

$$F(\tau) \sim \tau^{\alpha}, \tag{11}$$

where α is the scaling exponent.

A typical curve obtained from the detrended-fluctuation analysis of a signal is shown in Fig. 3(b).

3.3 Minimal-Cover Analysis

This method has been recently introduced [7]. It relates the minimal area necessary to cover a given plane curve in a specified scale to a power law behavior. The scale is introduced by dividing the domain of definition of the function in L intervals of width τ. A rectangle of base τ and height A_j can be associated to each interval j $(1 \le j \le L)$, and defines as

$$A_j = \max\{y_i, i \in [j, j+\tau]\} - \min\{y_i, i \in [j, j+\tau]\} \tag{12}$$

such that the minimal area will be given by

$$S(\tau) = \sum_{j=1}^{n} \tau A_j. \tag{13}$$

In the scaling region, $S(\tau)$ should behave as

$$S(\tau) \sim \tau^{1-\mu}, \tag{14}$$

where μ measures the fractality of the curve and is equal to zero when the signal presents no fractality.

A typical curve obtained from the minimal-cover analysis of a signal is shown in Fig. 3(c).

3.4 Box-Counting Analysis

The box-counting dimension is one of the best known fractal dimension [8] which can be easily defined and obtained numerically. It can be introduced in a general d-dimensional Euclidean space, where a hyper-volume is embedded, by considering the number of hypercubes of side length τ, $N_B(\tau)$, necessary to cover the entire volume. For a real fractal, $N_B(\tau)$ should follow the power law

$$N_B(\tau) \sim \tau^{-D_B} \tag{15}$$

where D_B is the box-counting fractal dimension.

For non-fractal objects, this dimension corresponds to the topological dimension and, in particular, for continuous planar curves, D_B is equal to 1.

A typical box-counting curve for a signal with n points is shown in Fig. 3(d).

4 Pattern Recognition Methods

In order to classify the vectors obtained from the application of statistical fluctuation and fractal analysis of ultrasonic signals techniques, four different pattern recognition techniques have been used, namely: principal component analysis, Karhunen-Loève transformation, neural network and Gaussian classifier. It is noteworthy that no noise suppression technique has been applied to the backscattered signals. The preprocessing techniques used are not very sensitive to noise, therefore, within our approach noise does not play an important role.

In order to make the paper self-contained, a brief discussion of each technique will be presented below.

4.1 Principal Component Analysis

Given a set of N column d-dimensional vectors $\{\mathbf{x}_i\}$ generated during Hurst analysis, detrended-fluctuation analysis, minimal cover analysis and box-counting analysis, the principal component analysis (PCA) technique works by projecting the vectors onto the directions defined by the eigenvectors of the group-covariance matrix $\mathbf{S}$, defined as

$$\mathbf{S} = \frac{1}{N}\sum_{i=1}^{N}(\mathbf{x}_i - \mathbf{m})(\mathbf{x}_i - \mathbf{m})^{\mathrm{T}}, \tag{16}$$

where $\mathbf{m}$ is the average vector,

$$\mathbf{m} = \frac{1}{N}\sum_{i=1}^{N}\mathbf{x}_i \tag{17}$$

and $\mathbf{T}$ denotes the vector transpose [9].

The projection along the direction of the eigenvector corresponding to the largest eigenvalue of $\mathbf{S}$ is the first principal component, and accounts for the largest amount of variation in the original vectors. The remaining principal components are arranged in decreasing order of the corresponding eigenvalues. It follows that the projection on the second largest eigenvector related to the second largest eigenvalue gives the second principal component [9].

4.2 Karhunen-Loève (KL) Transformation

Let $\mathbf{x}_i$ be the vector corresponding to the ith signal. The KL transformation [9] consists of initially projecting the training vectors along the eigenvectors of the within-class covariance matrix $\mathbf{S}_W$, defined by

$$\mathbf{S}_W = \frac{1}{N}\sum_{k=1}^{N_C}\sum_{i=1}^{N_k} y_{ik}(\mathbf{x}_i - \mathbf{m}_k)(\mathbf{x}_i - \mathbf{m}_k)^{\mathrm{T}}, \tag{18}$$

where N_C is the number of different classes, N_k is the number of vectors in class k, $\mathbf{m}_k$ is the average vector of class k, and $\mathbf{T}$ denotes the transpose of a matrix (in this case, of a

column vector). The element y_{ik} is equal to one if $\mathbf{x}_i$ belongs to class k, and zero otherwise. The resulting vectors are rescaled by a diagonal matrix built from the eigenvalues λ_j of $\mathbf{S}_W$. In matrix notation, this operation can be written as

$$\mathbf{X}' = \mathbf{\Lambda}^{-\frac{1}{2}}\mathbf{U}^{\mathrm{T}}\mathbf{X}, \tag{19}$$

where $\mathbf{X}$ is the matrix whose columns are the training vectors $\mathbf{x}_i$, $\mathbf{\Lambda} = \mathrm{diag}(\lambda_1, \lambda_2, \ldots)$, and $\mathbf{U}$ is the matrix whose columns are the eigenvectors of $\mathbf{S}_W$. This choice of coordinates assures that the transformed within-class covariance matrix corresponds to the unit matrix. Finally, in order to compress the class information, the resulting vectors are projected onto the eigenvectors of the between-class covariance matrix $\mathbf{S}_B$,

$$\mathbf{S}_B = \sum_{k=1}^{N_C} \frac{N_k}{N}(\mathbf{m}_k - \mathbf{m})(\mathbf{m}_k - \mathbf{m})^{\mathrm{T}}, \tag{20}$$

where $\mathbf{m}$ is the overall average vector. The full transformation can be written as

$$\mathbf{X}'' = \mathbf{V}^{\mathrm{T}}\mathbf{\Lambda}^{-\frac{1}{2}}\mathbf{U}^{\mathrm{T}}\mathbf{X}, \tag{21}$$

where $\mathbf{V}$ is the matrix whose columns are the eigenvectors of $\mathbf{S}_B$ (calculated from X').

4.3 Neural Network

In this study, statistical fluctuation and fractal analyses were used to process each ultrasonic signal, i, in order to generate a 25 component (or attribute) vector, $\mathbf{x}_i$. These vectors are used as inputs to the neural network. Geometrically, each input is represented by a point in a space of dimension 25, called space of inputs.

Nonlinear classifiers were implemented by a neural network with only one hidden layer of neurons totally connected. The optimized number of 3 neurons in the hidden layer was obtained after preliminary trial runs were carried out. A total of 3 neurons were used in the output layer, such that each class is distinguished by one neuron. Thus, the total number of synaptic weights in the network is 90 (78 weights between 25 input components plus a bias and 3 hidden layer neurons plus 12 weights between 3 hidden neurons plus a bias and 3 output layer neurons) whereas the number of training examples is 32 (80% of the vectors of each class), which satisfies Widrow's rule of thumb with accuracy up to three percent [10]. Logistic sigmoid activation functions were used in all the neurons.

Once defined the network architecture, adjustment of synaptic weights was performed by an error backpropagation learning algorithm [10, 11]. Input-target pairs are fed to the network, and following this supervised learning the output layer neuron producing the highest output corresponds to the selected class. The training was carried out at 1000 epochs, with a learning rate and with a moment equal to 0.1 and 0.75, respectively [10].

4.4 Gaussian Classifier

The Gaussian function is widely used as classifier of d-dimensional vectors, trained by supervised learning [9]. In general, the p-dimensional Gaussian function, for a given class i, is given by:

$$p(\mathbf{x}|\omega_i) = \frac{1}{(2\pi)^{\frac{p}{2}}|\mathbf{S}_i|^{\frac{1}{2}}} \exp\left\{-\frac{1}{2}(\mathbf{x} - \mathbf{m}_i)^{\mathrm{T}}\mathbf{S}_i^{-1}(\mathbf{x} - \mathbf{m}_i)\right\}, \tag{22}$$

where $\mathbf{S}_i$ is the covariance matrix associated to class i and $\mathbf{m}_i$ is the average vector also associated to class i, which are given respectively by (16) and (17), and $\mathbf{x}$ is an input vector. The maximum value of Gaussian function is observed for $\mathbf{x} = \mathbf{m}_i$ and the output of the function decreases with the increase of the distance between $\mathbf{x}$ and $\mathbf{m}_i$.

For each class, the average and covariance of the Gaussian function are calculated from the training set. Finally, the testing set is used to evaluate the performance of the Gaussian function in discriminating the vectors by choosing the highest output obtained from the different Gaussians associated to each class.

5 Results and Discussion

In the application of the analyses described above 40 backscattered signals associated to each cast iron microstructure have been used. With 3 possible classes, in the application of principal component analysis and Karhunen-Loève transformation, the fully-transformed vectors have $3 - 1 = 2$ relevant components [9]. However, in this work each vector $\mathbf{x}_i$ was associated with the class whose average vector was closest to $\mathbf{x}_i$ within the transformed three-dimensional space.

The vectors $\mathbf{x}_i$ have been built applying the different analyses and its components are given by (6), (11), (14) and (15). In all cases the vectors have been built with 25 components, and typical results obtained for the different analyses are shown in Fig. 3.

Except for the principal component analysis, where all vectors are classified into a single set, the results have been obtained by dividing the vectors into training and testing sets. The training set contains 80% of the vectors of each class, while the testing set contains the remaining 20%. The results presented for the different classification schemes correspond to an average taken over a 100 sets randomly built from 40 vectors for each class. This procedure ensures a good statistical significance. All relevant operations are performed as described above, and average classification success rate is calculated for both training and testing sets of signals.

Table 1 Percentage of vectors yielded from different analyses, which were correctly classified by applying the nearest-class-mean rule to the results of PCA

	RS	DFA	Minimal-cover	Box-counting
Lamellar	100.0	97.5	75.0	82.5
Vermicular	82.5	97.5	37.5	45.0
Nodular	92.5	100.0	77.5	75.0
Overall performance	91.67	98.33	63.33	67.5

The PCA results are presented in Table 1. As it can be seen, the best average classification, which was introduced by the nearest-class-mean rule, has been obtained by using RS and DF analyses. The results also show that, by combining the two analyses, a 100% average success rate classification can be achieved.

From Table 1 it is also possible to obtain the general performance of the combination of each statistical fluctuation analyses (Hurst analysis, detrended-fluctuation analysis) and principal component analysis (PCA) to discriminate between backscattered signals obtained from three classes of cast iron (lamellar, vermicular and nodular). The overall percentage found was 91.67% and 98.33% for RS and DFA, respectively, which is a reasonable result considering that a linear classifier without supervised learning was used.

Recently, Normando et al. [25] employed the combination of DFA (detrended-fluctuation analysis) and PCA (principal component analysis) to distinguish successfully between duplex stainless steel samples with different phase sigma percentage from backscattered ultrasonic signal and magnetic Barkhausen noise.

The results for the Karhunen-Loève classification, which was also introduced by the nearest-class-mean rule, are shown in Tables 2 and 3, for the training and testing sets respectively. In this case, a 100% average classification rate has been achieved for the testing and training sets by using RS and DF analyses. The worst results have been obtained by using minimal cover and box-counting analyses, where the 100% average classification rate has not been achieved for both sets. The overall worst result was obtained for the classification of the vermicular structure within the box-counting analysis.

Again, statistical fluctuation (DFA and RSA) combined with KLT (Karhunen-Loève transformation) was used in characterization of microstructural changes in coarse ferritic-pearlitic stainless steel [26]. A similar classification scheme was effectively used to classify electric steel samples with different heat treatment by means of magnetic hysteresis loops [27].

Results for the neural network classification scheme are shown in Tables 4 and 5, for the training and testing sets respectively. In this case, an average classification rate of almost 100% has been achieved at training regardless of the analysis method employed. However, for the testing set, as in the previous cases, average classification success rate of 100% has been reached by using RS and DF analyses only. The worst results have also been obtained by using the box-counting analysis, where the 100% average classification rate has not been achieved for both sets.

Finally, in Tables 6 and 7, we present the results for the Gaussian classification scheme, for the training and testing

Table 2 Average percentage of training vectors which were correctly classified by applying the nearest-class-mean rule to the results of KLT. Averages were taken over 100 sets of 32 training vectors, randomly chosen from a total of 40 vectors produced by different analyses

	RS	DFA	Minimal-cover	Box-counting
Lamellar	100.0	100.0	93.1	98.6
Vermicular	100.0	100.0	99.1	84.4
Nodular	100.0	100.0	99.1	94.4
Overall performance	100.0	100.0	97.1	92.47

Table 3 Average percentage of testing vectors which were correctly classified by applying the nearest-class-mean rule to the results of KLT. Averages were taken over 100 sets of 8 testing vectors, randomly chosen from a total of 40 vectors produced by different analyses

	RS	DFA	Minimal-cover	Box-counting
Lamellar	100.0	100.0	89.1	91.6
Vermicular	100.0	100.0	87.9	73.4
Nodular	100.0	99.8	94.0	86.8
Overall performance	100.0	99.93	90.33	83.93

Table 4 Average percentage of training vectors which were correctly classified by neural network. Averages were taken over 100 sets of 32 training vectors, randomly chosen from a total of 40 vectors produced by different analyses

	RS	DFA	Minimal-cover	Box-counting
Lamellar	100.0	100.0	100.0	100.0
Vermicular	100.0	100.0	100.0	99.8
Nodular	100.0	100.0	100.0	100.0
Overall performance	100.0	100.0	100.0	99.93

Table 5 Average percentage of testing vectors which were correctly classified by neural network. Averages were taken over 100 sets of 8 testing vectors, randomly chosen from a total of 40 vectors produced by different analyses

	RS	DFA	Minimal-cover	Box-counting
Lamellar	100.0	100.0	90.3	91.1
Vermicular	97.4	99.75	85.8	66.4
Nodular	100.0	100.0	91.1	79.8
Overall performance	99.13	99.92	89.07	79.10

sets respectively. In this case, although a 100% average classification rate has been achieved for the training set by using RS, DF and minimal cover analyses, it has not been reached for the testing set. The poorest result has been obtained by using any box-counting analysis and, even by considering the combination of the RS, DF and minimal cover analyses, the 100% average classification rate has not been achieved.

From results shown in Tables 1 to 7 it can be seen that, in general, lamellar and nodular microstructures have the best classification success rate. The classification of vermicular microstructure has the worst performance, indicating that this is the most difficultly separable class. The properties of cast iron are strongly dependent on its microstructure, which can be characterized by the elastic properties of the iron matrix and by the distribution in number, size and shape of the precipitated graphite particles. Since graphite of vermicular cast iron has the sphericity, average particle size and volume density intermediate values between nodular (ductile iron) and lamellar (grey iron), as well as most of its elastic properties, this may explain why this structure has the worst classification success rate. The samples studied in this work are the same ones used by Gao et al. in a previous work [28].

Table 6 Average percentage of training vectors which were correctly classified by Gaussian discriminator. Averages were taken over 100 sets of 32 training vectors, randomly chosen from a total of 40 vectors produced by different analyses

	RS	DFA	Minimal-cover	Box-counting
Lamellar	100.0	100.0	100.0	21.0
Vermicular	100.0	100.0	100.0	71.0
Nodular	100.0	100.0	100.0	70.9
Overall performance	100.0	100.0	100.0	54.3

Table 7 Average percentage of testing vectors which were correctly classified by Gaussian discriminator. Averages were taken over 100 sets of 8 testing vectors, randomly chosen from a total of 40 vectors produced by different analyses

	RS	DFA	Minimal-cover	Box-counting
Lamellar	98.8	100.0	85.9	18.8
Vermicular	78.9	95.4	60.3	62.0
Nodular	94.4	97.3	64.8	50.8
Overall performance	90.70	97.57	70.33	43.87

Results of quantitative metallography obtained from investigated cast iron samples are summarized in Table 8.

It can be seen that the average percentage of training vectors which were correctly classified (Tables 2, 4 and 6) is higher than the result for the test vectors (Tables 3, 5 and 7). This is because it is easier to classify a vector that was supplied to classifier during the training process. Even so, the results obtained for the test data, were very similar to the ones obtained for the training data, confirming their identification capability of the method to identify new signals. Lastly, it is possible that some error occurred during the classification may also be related to the low signal/noise ratio.

6 Conclusions

In this paper we applied two statistical fluctuation analyses, Hurst analysis and detrended fluctuation analysis, and two fractal analyses, minimal cover analysis and box-counting analysis, developed for the time series analysis, as preprocessing tools for the classification of different cast iron microstructures by using backscattered ultrasonic signals. The signals were obtained from samples containing three different microstructures, namely, lamellar, vermicular and nodular graphite. For the classification step, we employed principal component analysis and three assisted classification techniques, namely, Karhunen-Loève transformation, neural network classification scheme and a Gaussian classifier. In the application of the assisted classification techniques, 80% of the signals were used as a training set and 20% as testing set. In the classification scheme, for each class, 32 vectors were randomly selected for training and the remaining 8 vectors were used for testing. Aiming to ensure a good statistical significance, this training/testing procedure was repeated 100 times with different sets of randomly selected training and testing vectors. The results reported are averages taken over these 100 sets, and almost a 100% average success rate classification has been achieved for the training and testing sets in all classification schemes by combining the Hurst and DF analyses. The present results confirm previous ones [29–31], which show that the statistical fluctuation and fractal analysis combined with classification techniques for pattern recognition constitute a powerful tool when applied to ultrasonic measurements. Furthermore, in this case the technique was applied to backscattering signals obtained from pulse echo testing which the simplest ultrasonic nondestructive technique.

Table 8 Properties of graphite particles embedded in the investigated cast irons samples obtained by metallographic analysis by Gao et al. [28]

Property	Lamellar	Vermicular	Nodular
Particle diameter [μm]	71.90 ± 10.0	48.50 ± 3.2	35.01 ± 1.6
Sphericity	0.22 ± 0.01	0.39 ± 0.03	0.67 ± 0.02
Particle number density [10^{12} m^{-3}]	1.22 ± 0.30	1.76 ± 0.28	3.7 ± 0.44

Acknowledgements We acknowledged the financial support from the Brazilian agencies CNPq, FINEP (CT-PETRO) and CAPES, and from PETROBRÁS (Brazilian Oil Company).

One of authors gratefully acknowledges fruitful discussions with professors Igor Frota de Vasconcelos, Luiz Pereira Calôba and Guilherme de Alencar Barreto.

References

1. Sullivan, P.F., Papadakis, P.E.: Ultrasonic double refraction in worked metals. J. Acoust. Soc. Am. **33**, 1622–1624 (1961)
2. Vary, A.: Material property characterization. In: Moore, P.O. (ed.) Nondestructive Testing Handbook, Ultrasonic Testing, 3rd edn., vol. 7, pp. 365–431. ASTM, Columbus (2007)
3. Matos, J.M.O., de Moura, E.P., Krüger, S.E., Rebello, J.M.A.: Rescaled range analysis and detrended fluctuation analysis study of cast irons ultrasonic backscattered signals. Chaos Solitons Fractals **19**, 55–60 (2004)
4. Kantz, H., Schreiber, T.: Nonlinear Time Series Analysis, 1st edn. Cambridge University Press, Cambridge (1997)
5. Hurst, H.E.: Long-term capacity of reservoirs. Trans. Am. Soc. Civ. Eng. **116**, 770–808 (1951)
6. Peng, C.K., Buldyrev, V., Havlin, S., Simmons, M., Stanley, H.R., Goldberger, A.L.: Mosaic organization of DNA nucleotides. Phys. Rev. E **49**, 1685–1689 (1994)
7. Dubovikov, M.M., Starchenko, N.V., Dubovikov, M.S.: Dimension of minimal cover and fractal analysis of time series. Physica A **339**, 591–608 (2004)
8. Addison, P.S.: Fractals and Chaos: An Illustrated Course, 1st edn. IOP, London (1997)
9. Webb, A.R.: Statistical Pattern Recognition, 2nd edn. Wiley, West Sussex (2002)
10. Haykin, S.: Neural Networks, a Comprehensive Foundation, 2nd edn. Macmillian College, New York (1994)
11. Wasserman, P.D.: Neural Computing Theory and Practice, 1st edn. Van Nostrand Reinthold, New York (1989)
12. Telesca, L., Lapenna, V., Macchiato, M.: Mono- and multi-fractal investigation of scaling properties in temporal patterns sequences of seismic sequences. Chaos Solitons Fractals **19**, 1–15 (2004)
13. Kurnaz, M.L.: Detrended fluctuation analysis as a statistical tool to monitor the climate. J. Stat. Mech. Theor. Exp. P07009 (2004)
14. Govindan, R.B., Kantz, H.: Long-term correlations and multifractality in surface wind speed. Europhys. Lett. **68**, 184–190 (2004)
15. Carbone, A., Castelli, G., Stanley, H.E.: Time-dependent Hurst exponent in financial time series. Physica A **344**, 267–271 (2004)
16. Jennings, H.D., Ivanov, P.C., Silva, P.C., Viswanathan, G.M.: Variance fluctuations in nonstationary time series: a comparative study of music genres. Physica A **336**, 585–594 (2004)
17. Dutta, D., Barat, P.: Fractal characterization of ultrasonic backscattered signals from single crystal and pollycrystalline materials. J. Acoust. Soc. Am. **98**, 938–942 (1995)
18. Loper, C.R. Jr., Lalich, J.M., Park, H.K., Gyarmaty, A.M.: The relationship of microstructure to mechanical properties in compacted graphite cast irons. Am. Foundrymen's Soc. Trans. **88**, 313–330 (1980)
19. Liu, P.C., Loper, C.R., Kimura, T., Park, H.K.: Observations on the graphite morphology in cast irons. Am. Foundrymen's Soc. Trans. **88**, 97–118 (1980)
20. Murthy, V.S.R., Seshan, S.: Characteristics of compacted graphite cast iron. Am. Foundrymen's Soc. Trans. **92**, 373–380 (1984)
21. Itofuji, H., Kawano, Y., Inoyama, N., Chang, B., Yamamoto, S.: Am. Foundrymen's Soc. Trans. **91**, 831–840 (1983)
22. Nelson, J.A.: Cast irons. In: ASM Handbook Committee (eds.) Metallography and Microstructures, 9th edn., vol. 9, pp. 242–255. The Materials Information Society, New York (1985)
23. Silk, M.G.: Sizing crack like defect by ultrasonic means. In: Sharpe, R.S. (ed.) Research Techniques in Nondestructive Testing, vol. III, pp. 51–79. Academic Press, London (1977)
24. de Moura, E.P., Vieira, A.P., Irmão, M.A.S., Silva, A.A.: Applications of detrended-fluctuation analysis to gearbox fault diagnosis. Mech. Syst. Signal Process. **23**, 682–689 (2009)
25. Normando, P.G., Moura, E.P., Souza, J.A., Tavares, S.S.M., Padovese, L.R.: Ultrasound, eddy current and magnetic Barkhausen noise as tools for sigma phase detection on a UNS S31803 duplex stainless steel. Mater. Sci. Eng. A **527**, 2886–2891 (2010)
26. Padovese, L.R., da Silva, F.E., de Moura, E.P., Gonçalves, L.L.: Characterization of microstructural changes in coarse ferritic-pearlitic stainless steel through the statistical fluctuation and fractal analyses of Barkhausen noise. In: 36th Annual Review of Progress in QNDE, vol. 29. AIP Conference Proceedings, vol. 1211, pp. 1293–1300 (2010). New York
27. Silva, F.E., Freitas, F.N.C., Abreu, H.F.G., Gonçalves, L.L., de Moura, E.P., Silva, M.R.: Characterization of the evolution of recrystallization by fluctuation and fractal analyses of the magnetic hysteresis loop in a cold rolled non-oriented electric steel. J. Mater. Sci. **46**, 3282–3290 (2011)
28. Gao, W., Glorieux, C., Kruger, S.E., de Rostyne, K.V., Gusev, V., Lauriks, W., Thoen, J.: Investigation of the microstructure of cast iron by laser ultrasonic surface wave spectroscopy. Mater. Sci. Eng. A **313**, 170–179 (2001)
29. Tesser, J.A., Lopes, R.T., Vieira, A.P., Gonçalves, L.L., Rebello, J.M.A.: Fractal analysis of weld defect patterns obtained by radiographic tests. In: 33rd Annual Review of Progress in QNDE, vol. 26. AIP Conference Proceedings, vol. 894, pp. 539–545 (2007). New York
30. Vieira, A.P., de Moura, E.P., Gonçalves, L.L., Rebello, J.M.A.: Characterization of welding defects by fractal analysis of ultrasonic signals. Chaos Solitons Fractals **38**, 748–754 (2008)
31. Vieira, A.P., Vasconcelos, H.H.M., Gonçalves, L.L., Miranda, H.C.: Fractal analysis of metal transfer in MIG/MAG welding. In: 35th Annual Review of Progress in QNDE, vol. 28. AIP Conference Proceedings, vol. 1096, pp. 564–571 (2009). New York